BRAIN COMMUNICATIONS

Individualized phenotyping of functional amyotrophic lateral sclerosis pathology in sensorimotor cortex

Avinash Kalyani,[1,2,3,4] Alicia Northall,[1,5] Stefanie Schreiber,[2,6] Jascha Brüggemann,[7] Stefan Vielhaber,[6] Marwa Al Dubai,[6] Abrar Bin Ramadan,[6] Hendrik Mattern,[2,7,8] Oliver Speck,[2,7,8,9,10] Christoph Reichert[9] and Esther Kuehn[1,3,4,8]

Amyotrophic lateral sclerosis (ALS) is a progressive neurodegenerative disease characterized by the loss of motor neurons in primary motor cortex, leading to muscle weakness, atrophy and death within a median of 3 years. Even though ALS is characterized by different disease subtypes affecting different body parts, individualized phenotyping of functional ALS pathology has so far not been achieved. We recorded 7 Tesla functional MRI data while ALS patients and matched controls moved affected and non-affected body parts in the MR scanner. We applied robust Shared Response Modelling for capturing ALS-specific shared responses for group classification, and Partial Least Squares regression for relating the latent variables to clinical subtypes and the degree of disease progression. We show that disease onset and severity can be best modelled by functional connectivity rather than local activation changes. We also show that functional disease-defining information in primary motor cortex is not the strongest in the area that is behaviourally first-affected, deviating from the behavioural phenotype of the patients. When computing the model's weight distribution of the King stage classification and projecting them back into voxel space, the highest mean weights are present in the foot and tongue/face regions. Our data highlight the importance of 7 Tesla functional MRI task-based functional connectivity measures for classifying ALS patients in addition to structural readouts and provides evidence that a 7 Tesla functional MRI can be used for identifying a disease signature of each individual ALS patient.

1 Institute for Cognitive Neurology and Dementia Research (IKND), Otto-von-Guericke University Magdeburg, Magdeburg 39120, Germany
2 German Center for Neurodegenerative Diseases (DZNE), Magdeburg 39120, Germany
3 Hertie Institute for Clinical Brain Research (HIH), Tübingen 72076, Germany
4 German Center for Neurodegenerative Diseases (DZNE), Tübingen 72076, Germany
5 Nuffield Department of Clinical Neurosciences, University of Oxford, Oxford OX3 9DU, United Kingdom
6 Clinic for Neurology, Otto-von-Guericke University Magdeburg, Magdeburg 39120, Germany
7 Department Biomedical Magnetic Resonance (BMMR), Otto-von-Guericke University Magdeburg, Magdeburg 39120, Germany
8 Center for Behavioral Brain Sciences (CBBS) Magdeburg, Magdeburg 39120, Germany
9 Leibniz Institute for Neurobiology (LIN), Otto-von-Guericke University Magdeburg, Magdeburg 39120, Germany
10 Research Campus STIMULATE, Otto von Guericke University Magdeburg, Magdeburg 39106, Germany

Correspondence to: Avinash Kalyani
Hertie Institute for Clinical Brain Research
Otfried-Müller-Straße 27, Tübingen 72076, Baden-Württemberg, Germany
E-mail: avinash.kalyani@uni-tuebingen.de

Keywords: amyotrophic lateral sclerosis; PLSR; sensorimotor cortex; 7T-fMRI; disease progression

Received January 15, 2025. Revised January 14, 2026. Accepted April 8, 2026. Advance access publication April 9, 2026

Graphical Abstract

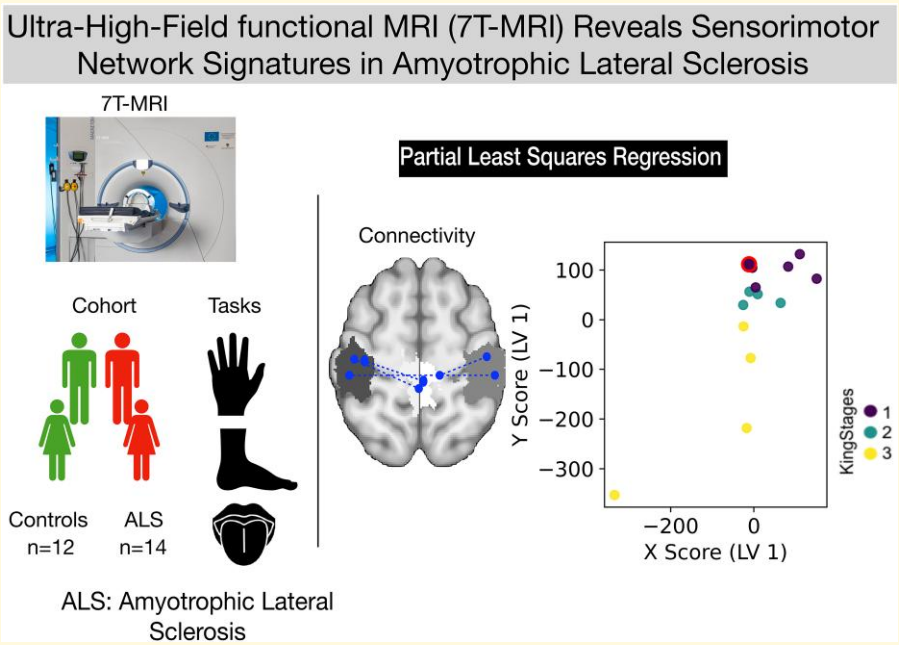

Introduction

Amyotrophic lateral sclerosis (ALS) is the most common form of motor neuron disease. It is characterized by progressive muscle weakness and atrophy, ultimately leading to death with a median survival time of 3–5 years from disease onset.[1,2] Both upper and lower motor neuron degeneration contribute to the classical ALS phenotype, while some patients present with a specific motor neuron phenotype. Behaviourally, ALS presents with a topographic disease phenotype, in which symptoms initially present focally in one body part. This onset is highly varied between patients, with roughly equal numbers experiencing onset in the head/face area (bulbar onset), the arms and hands (upper limb onset), or the legs and feet (lower limb onset).[3] According to the current dominant view, the disorder then progressively spreads to other body parts over the course of the disease, typically ending with bulbar and respiratory involvement.[4] A functional signature of ALS in affected sensorimotor cortex, however, is so far lacking.

This topographic disease profile is partly reflected by microstructural alterations in the primary motor cortex (MI) that can be described *in vivo*. Using 7T-MRI, a recent study showed that iron accumulation in the deeper layers of MI is the highest in the area that represents the first affected body part.[5] However, other microstructural changes, such as calcium accumulation in upper layers, appear atopographic in MI.[5] In addition, low-myelin borders that usually separate major body part representations in MI and hence are always located between two body part regions[5,6] show early calcium accumulation and also degenerate early in ALS,[5] which may speak against a strictly topographic disease profile. Despite its clinical significance, the individual functional topographic and/or atopograhic signature of ALS patients has not been described in great detail. This is a critical limitation, as the functional signature of ALS in the sensorimotor cortex is expected to show a clear relationship to behavioural impairments and disease spread and may more dynamically respond to treatments compared to structural measures. For instance, studies have shown that disruptions in functional connectivity can be detected before significant structural changes are observed in the brain.[7] This pattern has been noted in various neurodegenerative conditions, including Alzheimer's disease and Parkinson's disease, where early functional impairments can serve as indicators of subsequent structural degeneration.[8] Understanding these functional signatures could allow for monitoring disease progression or the effectiveness of new medications with clear functional output metrics. However, to achieve this, we first need a clear understanding of the functional signature of ALS in the human sensorimotor system, which is so far lacking.

Recent advances in neuroimaging techniques, particularly 7T-fMRI, have provided new avenues for describing small-scale circuits of the sensorimotor system in living participants and patients.[9,10] Compared to standard 3T-fMRI, 7T-fMRI offers higher spatial and temporal resolution, providing images of functional brain networks and topographic activation that are more precise,[11] which allows detecting subtle changes in brain activity that might otherwise be missed. Additionally, the shortened T2 relaxation rates at higher field strengths, such as 7T, improve the sensitivity of BOLD fMRI, making it especially beneficial for capturing fine-grained neural dynamics and subtle differences in activation patterns. These advantages make 7T-fMRI a powerful tool for studying neurodegenerative diseases like ALS, where early and localized changes in brain function are critical for understanding disease

progression. Moreover, since ALS patients often have difficulties remaining still for extended time periods, the ability of 7T-fMRI to obtain high-quality images in a shorter amount of time is a significant advantage, making it a superior choice for studying the intricate neural correlates of ALS. Nevertheless, few studies have employed 7T-MRI for studying MI pathology in a group of ALS patients, and most are confined to structural measures.[5,12-14] The few functional 7T-MRI studies that exist only measured resting state activation but did not probe the sensorimotor cortex when in action[15] and leave it open which functional variables best reflect disease progression.[16]

7T-fMRI patient studies come with their own set of challenges. One key challenge is to extract ultra-high resolution functional time series at the single patient level that represents the mesoscale architecture of the task representations but to nevertheless conduct group statistics to compare a single patient's profile to average functional patterns, as well as to clinical variables. Such computations require advanced statistical and computational methods that allow preserved resolution at the single patient level, in addition to comparing extracted functional patterns across patients. While univariate methods [e.g. voxel-wise t-tests or general linear models (GLMs)] are widely used and valuable in many fMRI studies, they often lack the sensitivity to detect distributed and subtle alterations in functional organization particularly in small, heterogeneous clinical cohorts and high-dimensional 7T data.

To address these challenges and to take full advantage of the ultra-high-resolution images, we aimed to employ techniques that can effectively handle high-dimensional fMRI datasets, namely robust Shared Response Modelling (rSRM)[17,18] and Partial Least Square Regression (PLSR).[19,20] We used the former (i.e. rSRM) to capture group specific shared neural responses for classifying ALS versus control participants, and the latter (i.e. PLSR) to identify the functional architecture of ALS that is associated with disease progression.

rSRM is a multivariate method designed to capture shared neural patterns across subjects, even in the presence of individual variability.[18] Unlike traditional alignment approaches, rSRM identifies a low-dimensional shared space that represents common neural responses, while discarding individual-specific components, such as noise or anatomical differences. This makes rSRM particularly suited for ultra-high field (7T) fMRI data, where inter-subject variability can obscure shared functional signatures. By aligning neural responses across groups, rSRM enables direct comparisons of functional architectures, such as those observed in ALS patients versus controls, and enhances the detection of group-specific patterns relevant to disease classification.

PLSR, on the other hand, is a multivariate regression method suited for high-dimensional data that has been widely used across disciplines such as social science, bioinformatics and neuroscience.[19,21,22] PLSR projects the functional response and the covariables (i.e. measures of disease progression) into a new space formed by its latent variables. To target the question of the a/topographic profile of functional markers, we used functional activation triggered by body part movements (hands, feet, lip/tongue) as well as the associated network centrality [i.e., Eigenvector centrality mapping (ECM)[23]], while, we used different markers of ALS disease progression measured by neurologists (i.e. ALSFRS-R, PUMNS) as covariables. In addition, we tracked functional changes of a subset of patients over time. Given PLSR can handle high-dimensional data, it is an ideal method for extracting relevant features from complex 7T-fMRI data, and for computing relationships between feature dimensions and behavioural as well as clinical profiles.[19-21,24] Combining these approaches provides valuable insights into the functional signature of the disease across different topographic locations and disease stages.

Specifically, using 7T-fMRI, we tested if (1) participants can be successfully classified into ALS patients versus controls based on their functional profile of the sensorimotor cortex recorded during body part movements, (2) there are latent variables in the functional time series that reflect disease severity and site of onset, and if so, if they become most evident in functional activation or functional connectivity changes and (3) disease-defining functional information is specific to the first-affected location in the sensorimotor cortex (i.e. topographic, reflecting the iron accumulation) or not specific to the first-affected location in the sensorimotor cortex (i.e. atopographic, reflecting the calcium accumulation and the early affected low-myelin borders), and whether there is any location in MI that is highly predictive of the severity of the disorder irrespective of onset site. The results of our study contribute to a deeper understanding of the neural mechanisms underlying ALS and offer potential functional neuronal signatures that characterize the disease for future clinical applications.

Methods

An overview of the methodologies applied and the experimental approach is depicted in Fig. 1.

Participants

We acquired fMRI data from $n = 14$ ALS patients (6 females, age: mean = 56.07 years, SD = 15.62 years) and $n = 12$ matched healthy controls (6 females, age: mean = 61.1 years, SD = 11.9 years). The patients were recruited from the University Hospital Magdeburg, Jena and Dresden and participated in the study between June 2018 and January 2024. The patients were first scanned after their first diagnosis of ALS. Controls were individually matched to a subset of 12 of the patients based on age [±2 years; $t(22) = -0.15$, $P = 0.883$], handedness, gender and years of education [±4 years; patients: mean = 14.5 years, SD = 2.7 years; controls: mean = 15.4 years, SD = 2.7 years; $t(22) = -0.82$, $P = 0.422$]. For two patients, matched controls could not be acquired due to a scanner software upgrade (from syngo MR B17 to VE12U) that occurred during the data collection period, which could have introduced inconsistencies in data comparability. Participants and patients underwent one 7T-MRI scan as well as behavioural assessments. Clinical assessments were performed by an experienced neurologist with the patients only. Among the patients, $n = 8$ had upper limb onset, $n = 3$ had lower limb onset and $n = 3$ had a bulbar onset (considered bilateral, see Table 1). $n = 3$ patients were scanned a second (and third) time to allow tracking of disease progression (P1: after 5 months, P6: after 7 months, P4: after 8 months, after 2 years and 4 months). Healthy matched controls were recruited from the

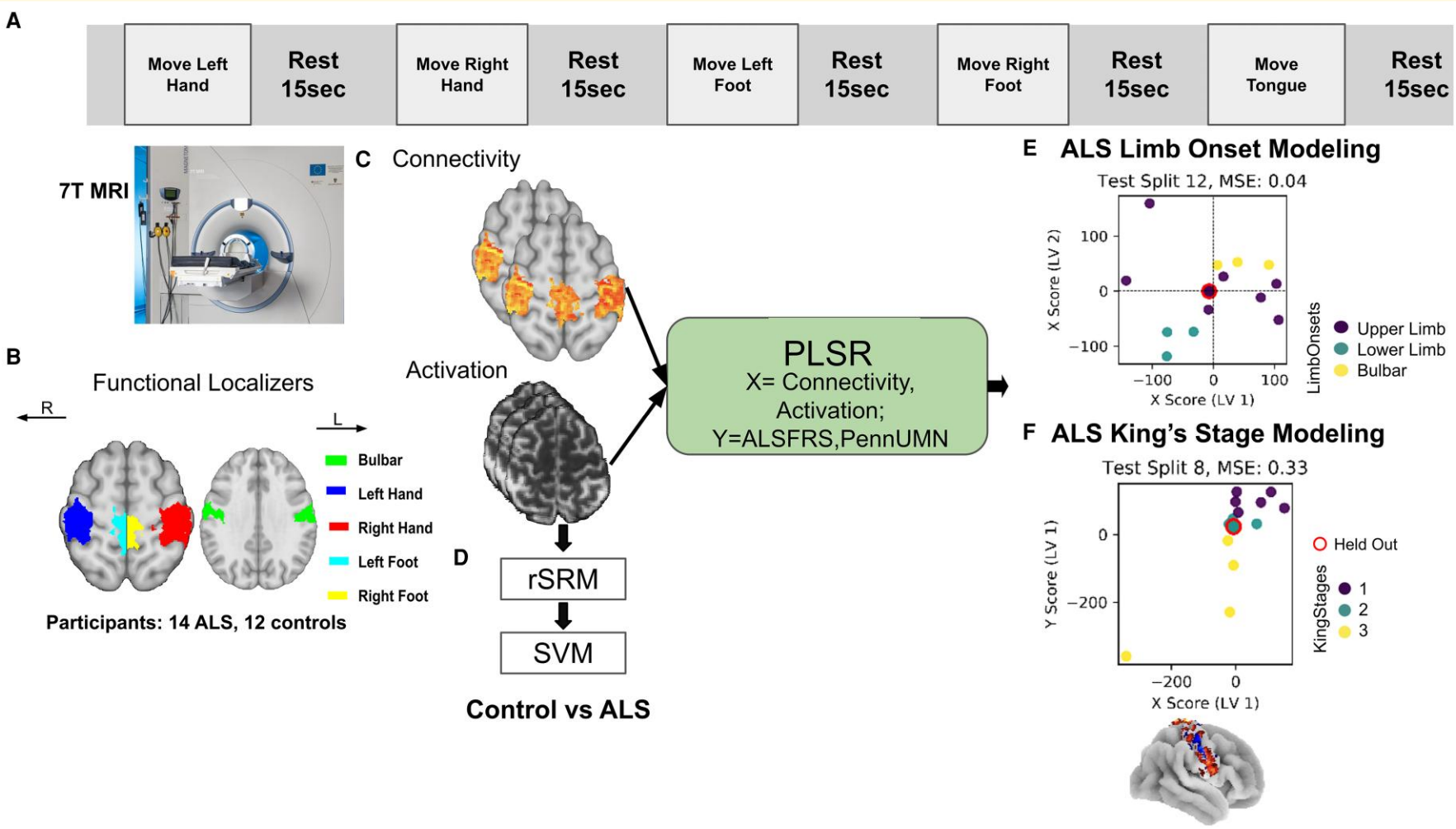

Figure 1 Experimental design and methodology. (**A**) During 7T-MRI scanning, participants and patients with a diagnosis of ALS were asked to move different body parts (left hand, right hand, left foot, right foot and tongue/lip), each movement lasting 12 s, followed by a 15 s rest period. **(B)** Functional localizers identify sensorimotor cortices activated by these movements: red for right hand, blue for left hand, cyan for left foot, yellow for right foot, green for tongue/face. **(C)** Connectivity and activation maps are generated from 7T-fMRI data, highlighting brain regions involved in the tasks. **(D)** Classification of ALS patients versus controls using robust Shared Response Modelling (rSRM) and Support Vector Machines (SVM) classification obtained from functional patterns. **(E)** Projections of ALS subjects using PLSR, with connectivity and activation as predictors (X) and ALSFRS and PUMNS as outcomes (Y). The scatter plot illustrates the latent variables (LV1 and LV2) for an example subject, showing clustering based on onset type (upper limb, lower limb, bulbar), with an MSE of 0.04. **(F)** ALS King's stage clustering is similarly conducted using PLSR, with scatter plots depicting the relationship between the X and Y scores in the latent variable space, highlighting the clustering of subjects according to King's stages (1, 2 and 3), with an MSE of 0.33. (The MRI scanner image shown in panel (A) was acquired at the MRI facility of Otto von Guericke University Magdeburg (contact: mri@ovgu.de) and is reproduced with permission.)

Table 1 Clinical and demographic information on ALS patients.

Patient	Age	Gender	Matched control	Onset type	ALSFRS-R total	King's stage	PUMNS
P1[a]	50	F	Yes	UL	44	1	1
P2	74	F	Yes	LL	25	3	22
P3	36	M	Yes	LL	45	1	15
P4[a]	48	M	Yes	UL	37	2	2
P5	53	M	Yes	B	33	3	2
P6[a]	66	M	Yes	UL	41	2	3
P7	60	M	Yes	UL	40	1	11
P8	52	F	Yes	UL	42	2	16
P9	64	F	Yes	B	47	1	1
P10	77	F	Yes	UL	35	1	0
P11	72	F	Yes	B	46	1	1
P12	73	M	Yes	UL	34	2	9
P13	25	M	No	UL	33	3	7
P14	35	M	No	LL	17	3	12

Onset type reflects upper limb (UL), lower limb (LL), or bulbar (B) onset site. The ALS Functional Rating Scale-Revised (ALSFRS-R) indicates disease severity, where lower values indicate greater impairment, with subscores for fine, gross, bulbar motor and respiratory function. The King's stage indicates the stage of disease progression based on the ALSFRS-R score, where Stage 1 reflects the involvement of one body part and that a clinical diagnosis has taken place, while Stage 2 and Stage 3 reflect the subsequent involvement of second and third body parts, respectively. The Penn Upper Motor Neuron Scale (PUMNS) score indicates clinical signs of upper motor neuron involvement, with higher scores indicating greater impairment (mean = 6.92, SD = 7.46, range: 0–22). F, female; M, male; P, patient. [a]Patients scanned more than once.

DZNE database in Magdeburg, Germany, with exclusion criteria including sensorimotor deficits, neurological disorders and contraindications for 7T MRI. Note that the structural [MP2RAGE, Quantitative Susceptibility Mapping (QSM)] data of X patients and X controls was previously published.[5] All participants and patients provided written informed consent prior to being scanned and were compensated for their participation. The study was approved by the local Ethics Committee of the Medical Faculty of the University of Magdeburg.

7T MRI data acquisition

MRI data were collected using a 7T MRI scanner (Siemens Healthineers) equipped with a 32-channel head coil (Nova Medical Inc.) at Otto-von-Guericke University, Magdeburg, Germany. The scanner was operated in Research Mode as an Investigational Device, allowing access to advanced and non-clinical imaging protocols. In a single 7T-MRI session, we acquired whole-brain MP2RAGE images with a spatial resolution of 0.7 mm isotropic (sagittal slices), with a repetition time (TR) of 4800 ms, echo time (TE) of 2.01 ms, field of view (FOV) read of 224 mm, flip angles of 5°/3°, inversion times of 900/2750 ms and a bandwidth of 250 Hz/Px. Additionally, whole-brain functional images were obtained with a spatial resolution of 1.5 mm isotropic using an EPI gradient-echo blood oxygen level-dependent (BOLD) sequence comprising 81 slices, with a TR of 2000ms, TE of 25 ms, FOV read of 212 mm, interleaved acquisition, GRAPPA factor of 2 and a Simultaneous Multi-Slice (SMS) factor of 2.

Functional imaging encompassed a blocked design paradigm, comprising 12-s periods of body part movements (left/right foot: moving the toes, left/right hand: tapping the fingers, tongue/face: moving the tongue against the lip while having the mouth closed) interspersed with 15-s rest intervals (see[5] for more details). Participants underwent pre-scan training to familiarize themselves with the movements, and visual cues were provided within the scanner (grey background, black colour) to prompt specific movements (e.g. 'prepare left hand', 'move left hand'). Each movement was repeated four times, resulting in a single run of a total 20 trials. Fingerless braces were worn to minimize hand movements during scanning. We also acquired whole-brain, 0.5 mm isotropic resolution susceptibility-weighted (SWI) images in 10/14 patients (transversal slices, repetition time = 22 ms, echo time = 9 ms, field of view read = 192 mm, flip angle = 10°, bandwidth = 160 Hz/Px), as two patients could not be scanned any longer due to fatigue and discomfort (note that the SWI sequence was measured last). The total duration of the scanning session was ∼75 min.

Clinical assessments

The ALS Functional Rating Scale-Revised (ALSFRS) is a widely used tool to measure the severity of ALS, consisting of subscores for fine motor function, gross motor function, bulbar and respiratory function.[25] Lower total scores on the ALSFRS indicate greater disease severity and functional impairment. On average, the ALSFRS score for the patients in this study was 41.1 (SD = 5.7, range: 25–47).

The King's College (KC) Staging System categorizes the progression of ALS based on the ALSFRS score, offering a structured way to assess the involvement of different body regions over time. King's stage 1 consists of functional involvement of 1 central nervous system (CNS) region, while Stages 2 and 3 correspond to functional involvement of 2 and 3 CNS regions, respectively.[26,27] In this study, this categorization is referred to as *King's Stage*.

The PUMNS is a clinical measure used to assess signs of upper motor neuron involvement in ALS patients. It quantifies the degree of upper motor neuron impairment, with higher scores indicating greater impairment.[28] In this study, the PUMNS ranged from 0 to 22, with a mean score of 6.92 and a standard deviation (SD) of 7.46. This wide range reflects the variability in upper motor neuron involvement among the participants.

Pre-processing of fMRI data

The pre-processing, conducted in Statistical Parametric Mapping 12 (SPM12), included motion correction, smoothing with a

2 mm full-width at half maximum (FWHM) kernel and slice-time correction.[5] Co-registration with anatomical 7T MP2RAGE image was executed in ITK-SNAP (v3.8.0),[29] with manual adjustments based on anatomical landmarks as needed. For group-level analysis, we registered all subjects' anatomical and co-registered functional data to MNI space after skull-stripping using ANTs' standard 'antsRegistrationSyN.sh' script.[30] This script performs rigid, affine and SyN registrations to the MNI 152 template.[31,32]

Statistical analysis

Functional activation

Prior to statistical analysis, we subjected the fMRI time series to band-pass filtering within the frequency range of 0.01–0.1 Hz. In SPM12, a first-level GLM was then applied to produce t-statistic maps for each body part involved in the task (for example, left hand, right hand, left foot, right foot and tongue/face). This process creates subject-specific activations for cortical fields relevant to the disease, i.e. the left hand, the right hand, the left foot, the right foot and the face area.[5,33] These activation maps were then used as predictors in the model to categorize disease stages.

Generating functional localizer masks within the sensorimotor cortex

Further group-level analysis involved generating localizer masks from the registered task fMRI data to isolate the most significant 1500 voxels for each distinct body part using the t-maps generated from the GLM analysis. This approach ensured that all ROIs had the same size, and patients who performed movements with reduced speed and/or strength compared with the controls were not disadvantaged in the analysis. For combining masks across subjects, a more stringent approach was applied: masks for each body part were intersected across all subjects, retaining only voxels that were consistently active in every subject. The resulting combined mask was then refined by identifying the largest connected cluster within this intersection using a connected component analysis. This method ensured that only the most robust and consistently activated regions were included for each body part (hand, tongue/face and foot), focusing on areas that are most relevant to disease progression.

Functional connectivity analyses

For functional connectivity analyses, we used Eigenvector Centrality Mapping (ECM), which is an analysis technique that measures the influence of a brain region within the entire network by considering both the number and quality of its connections. In the context of neuroimaging, ECM identifies key brain regions that act as hubs in neural communication pathways and may likewise identify areas of reduced functional communication that characterize affected areas in MI in ALS patients. This method assigns higher centrality values to regions that are extensively connected to other well-connected regions, thus highlighting areas critical for information flow and integration across the brain.[34] Utilizing Lipsia,[35] we generated EC maps to visualize and quantify the centrality of each voxel within the brain network, defined by the combined functional localizer masks for all the movements (left and right hand, foot and tongue/face), facilitating the identification of neural hubs that may be crucial for disease progression. The EC map was used as the second predictor for categorizing the disease stages (besides the activity profile) to test which of the two reflect better disease severity and site of onset [see hypothesis (2)].

In addition, seed-based functional connectivity was assessed across functionally localized regions by selecting seeds based on t-maps specific to task conditions. Each seed, defined by a radius of five voxels, provides averaged time series signals, and a dot product correlation was performed by correlating these signals with the time series from other voxels within the combined localizer mask. The resulting correlation values were then used to create a correlation map, which was employed in the subsequent analysis. To evaluate changes in functional connectivity across different stages of ALS, we computed the differences in the dot product correlation values between ALS patients and control subjects, averaging the results over all subjects to obtain a distribution of connectivity changes across various body parts and disease stages.

Robust shared response modelling for amyotrophic lateral sclerosis versus control classification

rSRM is a data-driven method designed to capture shared patterns of neural activity across multiple subjects, even in the presence of intersubject variability. Unlike traditional approaches that may be affected by differences in brain anatomy or individual cognitive strategies, rSRM identifies a common low-dimensional shared space that aligns brain responses across participants. This method is particularly useful for fMRI studies, where variations in brain anatomy, noise and subject-specific factors can obscure the detection of common neural signatures. By focusing on group-level shared information, rSRM improves the robustness and sensitivity of analyses, making it well suited for tasks like group classification, especially in populations with high variability, such as patients with neurodegenerative diseases like ALS.

To distinguish between ALS patients and control subjects, we employed rSRM, creating two separate models to capture group-specific shared information. We refer to these models as rSRM_1 and rSRM_2, corresponding to the ALS and control groups, respectively. Our objective was to establish distinct shared spaces that encapsulate the unique neural activity patterns for each group. We trained rSRM_1 using functional data from the ALS group and rSRM_2 using data from the control group, ensuring that each shared space was optimized to capture the group-specific functional signatures in a leave-one-out cross validation manner. During training, we utilized task-based fMRI data masked for specific regions (e.g. hand, foot, tongue/face) to create the shared spaces.

For each test subject, the functional data was split into two parts after rearranging the fMRI time series to ensure synchronization across all subjects. The first half of the functional time series was treated as Run 1, and the second half as Run 2. Using the training data from these runs, we estimated the shared basis and individual components separately for both rSRM_1 and rSRM_2. The individual term was then discarded to focus solely on the shared group-specific features, thereby reducing individual variability and emphasizing shared patterns that are more likely to generalize across subjects (as shown in study by Kalyani *et al.*[17]).

Next, the test subject's test data were projected into both the ALS and control shared spaces using the basis learned during

training. This resulted in two sets of projected data one corresponding to the ALS group and the other to the control group. These projected datasets were concatenated and served as input features for the classifier. By transforming the test data into both shared spaces, we ensured that the classifier could leverage group-specific information to make predictions about whether a subject belonged to the ALS or control group. In the classification step, leave-one-subject-out cross-validation was employed, with the subject's group (ALS or control) serving as the class label. This process was repeated for all subjects in both groups, enabling the classifier to comprehensively learn patterns specific to each group while accounting for inter-subject variability. By discarding the individual term and focusing on the shared group-level information, our approach effectively utilized the distinct shared neural patterns in ALS and control subjects. This allowed us to improve classification performance by minimizing individual noise and emphasizing disease-specific features. For this binary classification task, the chance accuracy was set to 0.5, given the two distinct groups involved.

Control analyses: general linear model analysis for group comparison

To test whether also conventional univariate analysis methods can detect ALS-related alterations in sensorimotor cortex, we performed voxel-wise statistical analysis using the GLM as implemented in SPM12. For each participant, first-level GLM analyses were conducted to derive contrast estimates for the comparison between different body part movements (i.e. left hand movement versus other movements, right hand movement versus other movements similarly for left/right foot, and tongue). This was done after anatomical normalization to the MNI 152 template of SPM 12. These contrasts were then submitted to two second-level two-sample t-tests comparing ALS patients ($n = 12$) and healthy controls ($n = 12$) and vice versa. Group-level statistical maps were thresholded at $P < 0.001$ [corrected (FWE) and uncorrected], with a minimum cluster extent of 3 voxels.

Partial least squares regression analysis

In order to test whether there are latent variables in the functional time series that reflect disease severity and/or disease onset, and if so, whether they become more evident in functional activation patterns and/or functional connectivity changes, we used PLSR and computed the following steps: PLSR projects the response and the covariables into a new space formed by its latent variables by decomposing both X matrix (i.e. task activation, connectivity) and y (i.e. ALSFRS-R, UMN-Penn scores) of n (= 14) number of subjects into orthogonal scores and loadings. The general formulation is given by:

$$X = TP^T + F_X$$

$$Y = UQ^T + F_y,$$

where, $X = (x_1, \ldots . x_n)^T$, represents the predictor matrix comprising of fMRI time series data of n subjects; $Y = (y_1, \ldots . y_n)^T$, represents the response matrix i.e. behavioural data (in our case it is ALSFRS scores and UMN-Penn scores) . $T = (t_1, \ldots . t_L)$ and $U = (u_1, \ldots . u_L)$ are the (n × L) matrices of L latent components corresponding to X and Y, respectively. The (p × L) matrix P and the (q × L) matrix Q are loadings and the (n × p) matrix Fx and the (n × q) matrix Fy are the matrices of residuals. Since our objective is to perform least squares regression in a low-dimensional latent space, the underlying assumption is that the latent component ui can be well predicted from ti from a relation such as:

$$U = TD,$$

where, D is the (L × L) matrix. We need to maximize the covariance between t_i and u_i to satisfy the above assumption which produces weight matrices $W = (w_1, \ldots . w_L)$ and $C = (c_1, \ldots . c_L)$, the equation is given by:

$$max_{(t,u)}\ cov(t, u) = max_{(w,c)}\ cov(Xw, Yc),$$

Our first aim was to relate functional activation and connectivity patterns to clinical outcomes. Our second aim was to group patients according to their disease progression (i.e. King's Stages 1, 2 and 3), and the initial site of symptom onset (i.e. upper limb, lower limb and bulbar regions). To achieve these goals, we employed two distinct PLSR models in a leave-one-out (LOO) cross-validation manner, each tailored to different predictive tasks: estimating ALSFRS scores and PUMNS from ECM and functional activation.

We utilized ECM values derived from pre-processed fMRI time series data as the independent variable (X), and the ALSFRS scores obtained from the patient cohort as the dependent variable (Y) (see Fig. 1F). For modelling the PUMNS, we extracted fMRI time series data from the combined functionally localized masks specific to hand (i.e. both left and right hand regions), foot (i.e. both left and right foot regions), and tongue movements (i.e. bulbar region) together as the independent variable (X) and the PUMNS scores as dependent variable (Y) (see Fig. 1E).

We evaluated the model's performance by calculating MSE for each LOO cross-validation split. This assessment allowed us to project the test subject data onto the latent-variable space, facilitating an analysis of data clustering in relation to disease progression and symptom onset. For hypothesis (2), we used the response matrix Y, which included ALSFRS scores to predict the disease stage of ALS patients and UMN-Penn scores to predict the disease onset. For hypothesis (3), we projected the weights back into voxel space to determine if the weight distribution was topographic or atopographic. Topographic differences in region-wise weight distributions were evaluated using a one-way repeated-measures ANOVA, followed by Holm-corrected *post hoc* paired comparisons.

Control analysis: QSM- versus ECM-based PLSR

The patients tested here partly overlapped with a previously reported patient cohort where structural information was extracted to obtain disease-defining information in MI.[5] In order to test whether structural markers (QSM) and functional connectivity (ECM) capture overlapping or distinct disease-defining information in MI, we conducted a complementary PLSR analysis on

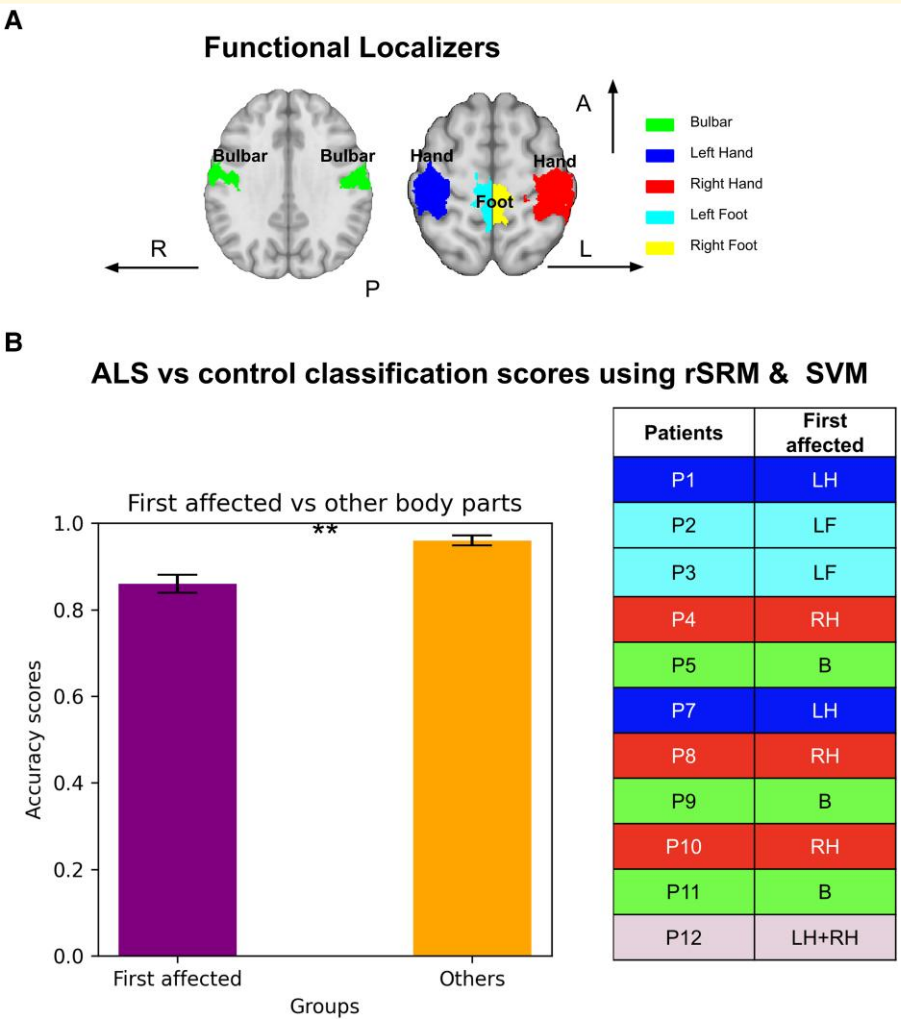

Figure 2 Classification of participants into patients versus controls based on functional activation in sensorimotor cortex: (**A**) Axial brain slices display regions-of-interest (ROIs) used for functional localization. Different colours indicate body parts: blue for left hand (LH), red for right hand (RH), light blue for left foot (LF), yellow for right foot (RF), green for tongue/face (bulbar region—B). (**B**) Bar plots show mean classification accuracy for ALS versus controls obtained using rSRM features and an SVM classifier with leave-one-subject-out cross-validation. Accuracies are grouped by features extracted from the first clinically affected body-part ROI (purple) versus non-first-affected ROIs (orange). The data represent the classification accuracy from one cross-validation fold (i.e. one held-out subject) within the corresponding ROI group. Bars show mean ± SEM across folds. Group differences were assessed using a two-sample *t*-test on fold accuracies [$t(120) = -3.92$, $P = 1.50 \times 10^{-4}$]. The table lists the first affected body part for each ($N = 12$) ALS patient.

two modalities QSM and ECM using data from the $n = 8$ patients for whom both readouts were available. Pre-processed QSM maps[5] were spatially normalized to the MNI-152 template used here (1 mm isotropic)[32] using ANTs' 'antsApplyTransforms' with the registration matrices generated in previous steps.

For each modality separately, we arranged the subject-by-voxel QSM or ECM values, respectively, into a predictor matrix X, and the corresponding ALSFRS-R scores into a response vector Y algorithm, decomposed the training set (X_train, Y_train) into latent scores (T,U) and loadings (P,Q), and projected the held-out subject into that latent space. Model accuracy was assessed by the mean squared error (MSE) on the left-out test fold. From each fold's first latent component (LV1), we extracted the absolute loadings within each ROI and averaged them across folds to produce modality-specific spatial profiles.

To examine how the first two components were distributed across our three ROIs at the single-subject level, we then trained separate two-component PLS models (PLS_2) for QSM and ECM and compared their LV1 and LV2 weight patterns within the hand, foot and tongue regions.

Per cent signal change analyses over time

As a final control analysis, we tested whether or not the strength of the recorded brain response is related to disease progression. We calculated per cent signal change for the subset of ALS patients ($n = 3$) who were measured more than once. Per cent signal change was

calculated using the rest condition averaged over the sensorimotor region of the brain within the two activity blocks as a baseline, and the task block as the parameter. This provides information about the change in brain activity as the disease progresses (data shown in Supplementary Fig. 2, Supplementary Table 1).

To mitigate the inherent variability in BOLD signal interpretation, we z-scored the voxel-level time series and applied band-pass filtering (0.01–0.1 Hz) before calculating per cent signal change. These pre-processing steps standardize the data, reduce noise and focus on task-relevant neural activity. However, it is important to note that BOLD remains a relative measure influenced by physiological and vascular factors, such as cerebrovascular reactivity and cerebral blood flow, which may still impact the interpretation of longitudinal changes.

Results

Successful classification of participants into patients versus controls based on functional activation in sensorimotor cortex

To investigate if (1) participants can be successfully classified into patients and controls based on their functional activation in the sensorimotor cortex, we extracted shared response patterns across the group using rSRM, and trained SVM for predicting group membership (i.e. patient, control). Successful group classification could be reached, with an overall classification accuracy of 0.91 ± 0.001 (mean ± SEM). To test if the classification is mainly based on the region of the first-affected body part, or on regions of behaviourally not yet affected or later affected body parts, we compared classification accuracies between first-affected and not-first-affected body parts. Results revealed that first affected regions show significantly lower classification accuracy as compared to non-first affected regions [first-affected: 0.86 ± 0.021, non-first affected: 0.96 ± 0.012, ($t(120) = -3.92$, $P = 1.50e\text{-}04$, see Fig. 2B]. The feature space driving this classification was further explored in an additional supplementary analysis (shown in Supplementary Fig. 5). Dimensionality reduction via principal component analysis and t-distributed stochastic neighbour embedding (t-SNE) revealed clearer group separation in the SRM-aligned space compared to raw time series, suggesting enhanced functional pattern distinctiveness through shared-response modelling (see Supplementary Figs 5A, B).

Additionally, to assess whether univariate methods could similarly discriminate between patients and controls, we conducted a complementary group-level analysis using SPM-based GLM contrasts. Despite modelling condition-specific BOLD responses for each movement and performing voxel-wise two-sample t-tests (control versus ALS and ALS versus control), no statistically significant activation differences survived correction for multiple comparisons. While uncorrected maps showed scattered sub-threshold group differences, these did not form coherent patterns (see Supplementary Fig. 1A and B). These results highlight the limited sensitivity of mass-univariate approaches in high-resolution datasets with subtle and distributed functional changes, reinforcing the value of multivariate methods such as rSRM and SVM for classification in ALS.

Identification of latent variables that reflect disease onset and severity

To test if (2) PLSR allows the identification of functional signatures that reflect disease onset and/or severity, and if so, if functional activation or functional connectivity changes are more sensitive to these clinical variables, we implemented PLSR using the functional activation and connectivity profiles as predictors, and related those to ALSFRS and PUMNS reflecting disease severity and onset. A combined localizer mask was used to derive data from different regions in MI (hand, foot, tongue), and the absolute values of the averaged model weights for each region were then plotted to assess their relative contribution to the overall modelling framework.

Modelling the disease onset

For functional activation, the overall average MSE was 1.02 ± 0.39 (mean ± SEM). The scatter plots in Fig. 3A depict the separation between ALS onset types based on functional activation (purple: upper limb onset, cyan: lower limb onset, yellow: bulbar onset) across six test splits. While LV1 successfully separates lower limb onset from bulbar onset, upper limb onset cannot clearly be identified. This is reflected in the results when calculating the classification for each topographic area separately: the tongue/face region (bulbar) shows the highest average weight (5.3 ± 0.1e−5), followed by the foot region (3.8 ± 0.1e−5) and the hand region with lowest weights (1.9 ± 0.1e−5, see Fig. 3). The histogram in Fig. 3C shows the distribution of MSE values across splits, with the majority of splits clustered below 3, indicating good predictive performance. However, a wider spread of MSE values, with some splits showing MSEs as high as 6, suggests more variability in model performance.

For functional connectivity, the overall MSE was 1.22 ± 0.43. The scatter plots in Fig. 3D show better clustering of onset types compared to the functional activation, particularly for lower limb versus bulbar onset along LV1. Unlike functional activation, upper limb onset is also more clearly separated in many of the splits (e.g. splits 4, 5, 10 and 12), resulting in a more distinct grouping of onset types in the latent variable space. This is reflected in the weights calculated per topographic area, where the hand region here shows higher weights (0.45 ± 0.1e−3). Highest weights, however, were still obtained from the tongue/face region (0.86 ± 0.1 e−3), followed by the foot region (0.79 ± 0.1e−3, see Fig. 3E). The histogram in Fig. 3F shows a consistent spread of MSE values, with most values concentrated between 1 and 3, and fewer outliers compared to functional activation. Together, these results show better and more consistent performance for functional connectivity-based classification compared to functional activation-based classification of onset site across splits.

Modelling disease severity

With respect to functional activation, the overall MSE is 1.22 ± 0.33 across all cross-validation splits. However, the model shows fluctuations in the LV space with respect to the projection of the subjects (see Fig. 4B). This indicates that there is instability in the

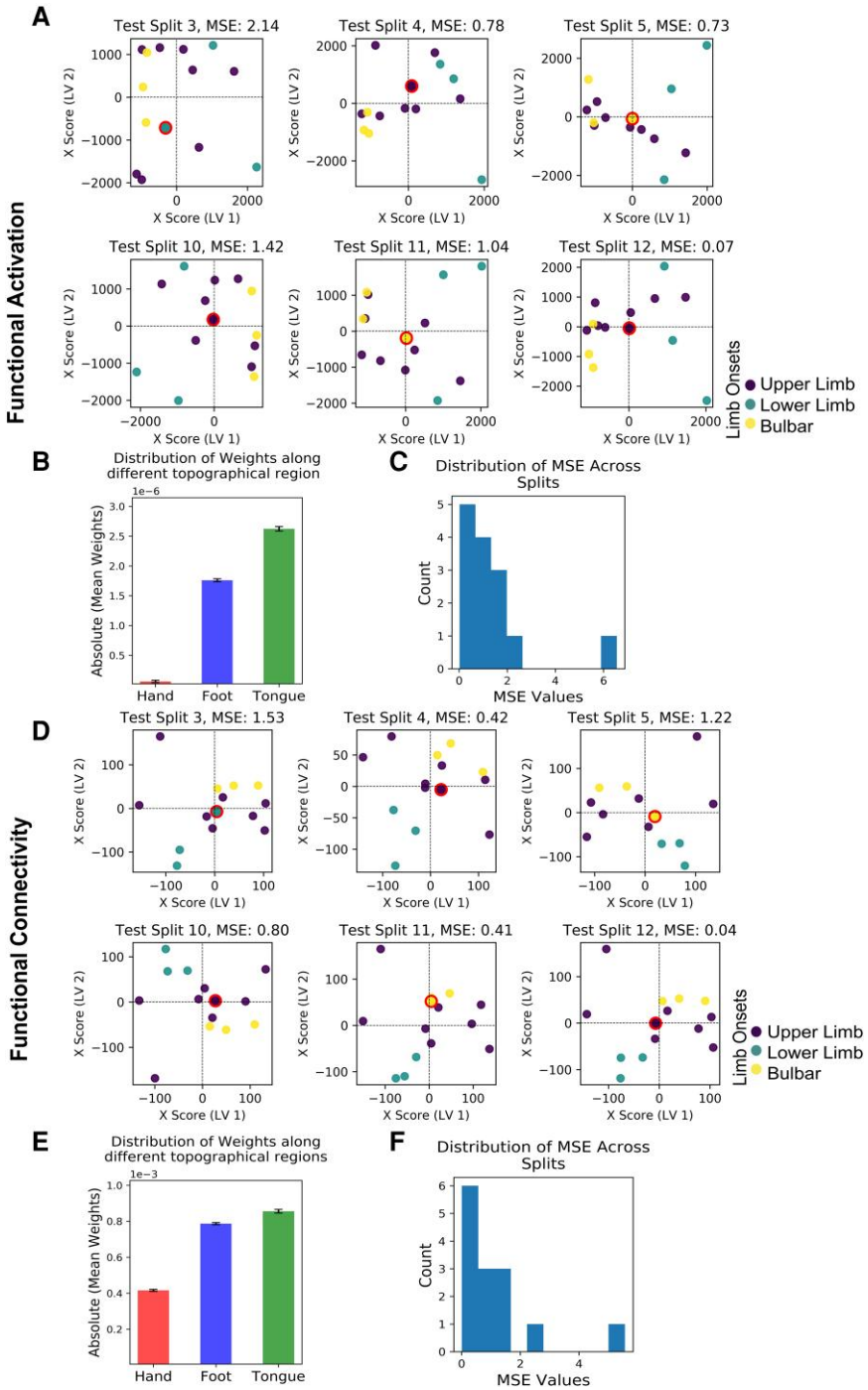

Figure 3 Modelling of ALS onset site based on fMRI data from sensorimotor cortex during body part movements. (**A**) + (**D**) Scatter plots depict the relationship between the first latent variable (LV1) and the second latent variable (LV2) for test subjects using PLSR, with different coloured circles representing the ALS onset classes (purple: upper limb onset, cyan: lower limb onset, yellow: bulbar onset). The position of each dot in the latent space represents an individual subject, with the colour indicating the onset class and the size reflecting the group distribution. Red-bordered dots indicate the held-out test subjects in each split. The Mean Squared Error (MSE) values shown in the subplot titles reflect the modelling error for each test case. (**A**) Projections for functional activation across 6 test splits, with MSE values provided for each split. (**B**) Bar plot summarizing the distribution of weights across topographical regions (hand, foot, tongue) for functional activation (N = 14 ALS patients). (**C**) Histogram showing the distribution of MSE values across test splits for functional activation, where each data point represents the MSE obtained for one held-out test subject (one cross-validation split). (**D**) Projections for functional connectivity across 6 test splits, with MSE values provided for each split. (**E**) Bar plot summarizing the distribution of weights across topographical regions (hand, foot, tongue) for functional connectivity (N = 14 ALS patients). (**F**) Histogram showing the distribution of MSE values across test splits for functional connectivity, with each data point corresponding to the MSE from one held-out test subject.

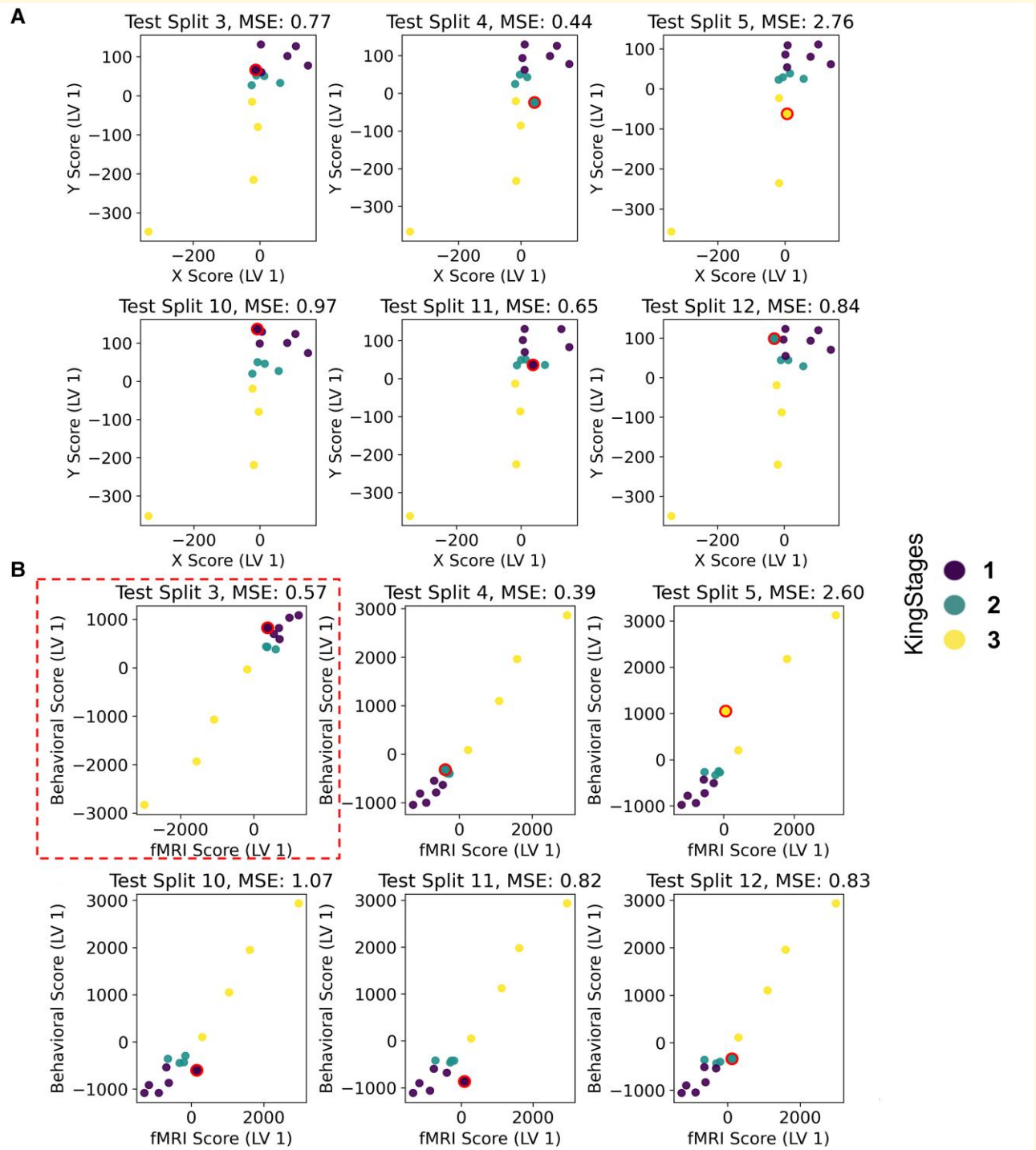

Figure 4 Modelling ALS king stage based on fMRI data of sensorimotor cortex during body part movements: scatter plots show the relationship between the predicted Y scores (disease stages) and the observed X scores (**A**—ECM, **B**—Brain activation) in the latent variable (LV) space for various test splits. The points with red circles represent the test subjects projected in the LV space. The colour coding of the points corresponds to the King stages: 1 (purple), 2 (blue) and 3 (yellow). The mean squared error (MSE) values shown for each test split provide an estimate of how well the model captures individual variation in the held-out subjects.

model, even though there is consistent grouping observed across all the splits. Consequently, this model was not investigated further.

With respect to functional connectivity, the averaged MSE is 1.40 ± 0.30 across all cross-validation splits. The model shows consistent performance in predicting ALSFRS scores from functional connectivity, i.e. EC (MSE range between 0.33 and 4.60 with four splits at MSE > 1, which indicates lower predictive power). Specifically, ECM LV1 reveals distinct groupings of

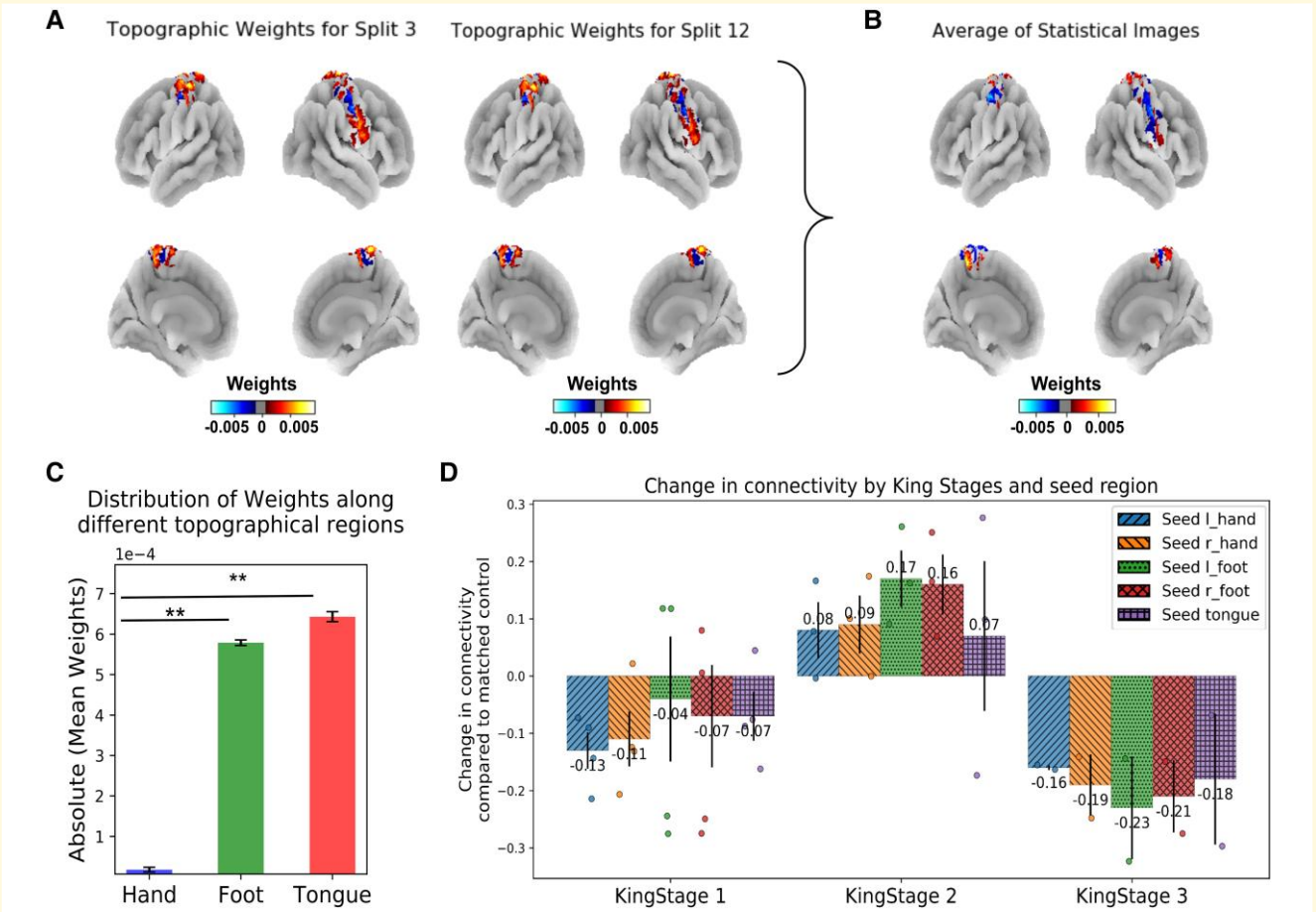

Figure 5 Topographic distribution: (**A**) Topographic weights for selected splits: Inflated cortices illustrate topographic distribution of weights derived from PLSR (for example test splits 3 and 12). Colour bars indicate weight values, with blue representing negative weights and red representing positive weights. These weights highlight cortical areas most associated with the ALS King stage for each test split. (**B**) Aggregated brain images show the average topographic weights across all test splits. This summary representation highlights the consistent brain regions associated with ALS progression, as indicated by the colour bar where blue gradient indicate negative weights (i.e. if the connectivity in these regions increase the ALSFRS scores decrease) and more red/yellow values indicate positive weights (i.e. increased connectivity patterns in this region relates to better ALSFRS scores). (**C**) Bar graph depicts the mean absolute PLSR weights distributed across different topographical regions (hand, foot, tongue/face) (N = 14 subjects; 14 data points per region). Error bars represent the standard error of the mean. A one-way repeated-measures ANOVA revealed a significant main effect of region on mean absolute weights [$F(2,26) = 14.20$, $P = 0.0001$]. *Post hoc* Holm-corrected paired comparisons showed significantly higher weights in the foot and tongue/face regions compared to the hand region (hand versus foot: $p_{holm} = 2.05 \times 10^{-6}$; hand versus tongue/face: $p_{holm} = 0.005$), while no significant difference was observed between the foot and tongue/face regions ($p_{holm} = 0.63$). **(D)** Bar graph shows the mean change in functional connectivity relative to matched controls (ALS—control) across ALS King's College disease stages (stages 1–3), shown separately for seed regions corresponding to left hand, right hand, left foot, right foot and tongue movements. Each dot represents an individual ALS—control connectivity difference value, and bars represent the mean across data points within each disease stage, with error bars indicating the standard error of the mean. The number of data points corresponds to the number of ALS and control comparisons contributing to each stage (N = 4 for stage 1, N = 3 for stage 2, N = 2 for stage 3).

participants according to their ALS King stages (1, 2 and 3). Participants in ALS King Stage 3 are consistently grouped below '0' on the *y*-axis, while participants in ALS King Stages 1 and 2 are grouped above '0' on the *y*-axis. This consistent grouping across different cross-validation splits suggests that the first latent variable of the functional connectivity profile effectively captures variability associated with ALS disease severity (see Fig. 4A). When projecting the test subject' data onto the latent variable space, data points fall within the same grouped regions as the training data points observed in the scatter plot (see Fig. 4, red outlined points). This confirms the model's ability to generalize and predict ALS disease stages based on connectivity (ECM) values, which has been less successful based on functional activation (see above).

To further explore the relationship between disease severity and different readouts, we conducted an exploratory multimodal analysis comparing functional connectivity (ECM) with structural susceptibility-based metrics (QSM) in a subset of $n = 8$ ALS patients where both modalities were available. Using separate PLSR

models for ECM and QSM features, we found that while both modalities were associated with clinical severity, they exhibited distinct latent variable structures and spatial emphasis. Specifically, ECM-derived latent variables showed more distributed contributions across hand and foot regions, whereas QSM-derived features were more strongly weighted towards the foot representation. These results suggest that functional and structural imaging capture complementary aspects of ALS-related cortical pathology (see Supplementary Figs 3 and 4).

To explore the network level effect further, Fig. 5D illustrates the averaged changes in functional connectivity across different ALS disease stages compared to matched controls, which presents as an inverted u-shaped profile: In King Stage 1, functional connectivity is decreased across all seed regions relative to controls, with reductions observed in all regions (left hand: −0.13, right hand: −0.11, left foot: −0.04, right foot: −0.07 and tongue: −0.07). In King Stage 2, an increase in connectivity can be observed in patients versus controls again for all regions (left hand: +0.08, right hand: +0.09, left foot: +0.17, right foot: +0.16 and tongue: +0.07). In King Stage 3, connectivity is again reduced in patients versus controls in all regions (left hand: −0.16, right hand: −0.19, left foot: −0.23, right foot: −0.21 and tongue: −0.18). See Supplementary Fig. 2 and Supplementary Table 1 for longitudinal data sampled from different time points available for $n = 3$ patients.

In summary, with respect to (1) and (2), we have shown that BOLD signal change in sensorimotor cortex during body part movements can be used to successfully classify a group of participants into patients versus controls, to classify patients with respect to disease severity and site of onset, and that functional connectivity is a better predictor for both disease onset and disease severity compared to functional activation. We further show that functional connectivity changes in patients versus controls present with an inverted u-shaped profile, with reduced connectivity in early disease stages, higher connectivity in middle disease stages, and a drop in connectivity in more severe disease stages.

Topographic versus atopographic profile

Finally, we investigated if (3) disease-defining functional information is specific to the first-affected topographic location in the sensorimotor cortex (i.e. topographic, reflecting the iron accumulation) or not specific to the first-affected topographic location in the sensorimotor cortex (i.e. atopographic, reflecting the calcium accumulation), and whether there is any topographic location in MI that is highly predictive of the severity of the disorder irrespective of onset site. Above, we have reported better classification accuracy in the patient versus control classification in regions of the behaviourally non-first affected body part compared to regions of the first-affected body parts. This shows that functionally disease-defining regions in MI are not strongest in the area that is behaviourally first-affected.

In addition, we observed higher weights in the foot and tongue regions compared to the hand region when modelling the association with the site of disease onset. To explore this effect of potentially more predictive areas in MI further, we computed the model's weight distribution (based on connectivity) of the King's Stage classification and projected them back into voxel space. In this way, the regions that drive the classification for disease severity can be identified precisely in MI. Results reveal that the highest mean weights are present in the foot and tongue/face regions, with the hand region showing marginally low weights (hand = 1.72e−05 ± 5.78e−06, foot = 5.7e−04 ± 6.828e−06, face = 6.4e−04 ± 1.22e−05, see Fig. 5C). A one-way repeated-measures ANOVA revealed a significant effect of topographic region on mean absolute weight distributions [$F(2,26) = 14.20$, $P = 0.0001$]. *Post hoc* Holm-corrected paired comparisons showed significantly higher weights in the foot and face regions compared to the hand region (hand versus foot: $p_{holm} = 2.05 \times 10^{-6}$; hand versus face: $p_{holm} = 0.005$), while no significant difference was observed between the foot and face regions ($p_{holm} = 0.63$) (see Fig. 5C). This indicates that higher connectedness (i.e. centrality) in the face and lower limb regions within the brain's network is predictive of the King stage of the disease, whereas this is less the case for the hand region. Both for the modelling of disease onset and disease severity, the foot and face areas show the highest predictive power, whereas the hand area shows lowest predictive power.

Discussion

ALS is a rapidly progressing neurodegenerative disease characterized by the loss of motor control and associated changes in the cytoarchitectural architecture of MI.[1] Whereas previous studies mostly focused on structural alterations, the present study aimed to uncover the distinct functional activity signature of MI associated with ALS onset site and progression using ultra-high field 7T-fMRI, rSRM and PLS regression analysis. Our results (1) confirm that participants can be successfully classified into ALS patients and controls based on their BOLD signal change in sensorimotor cortex recorded during body part movements, (2) show that latent variables specifically of the functional connectivity maps (but less so of the functional activation maps) reflect disease severity and disease site of onset and (3) demonstrate that disease-defining functional information is not specific to the first-affected topographic field in sensorimotor cortex, but that the foot and face areas in MI are most predictive of the severity of the disorder irrespective of onset site. Comparative analyses between the structural data of a previous publication assessing an overlapping cohort of $n = 8$ patients further suggest that structural and functional analyses uncover complementary rather than overlapping aspects of the disease phenotype. The results of our study contribute to a deeper understanding of the cortical mechanisms underlying ALS, and offer a novel methodological approach to characterize the disease in future clinical studies.

We first show that ALS patients can be successfully distinguished from healthy controls based on functional activation in the sensorimotor cortex, with an overall classification accuracy of 0.91 ± 0.001. This aligns with previous studies showing distinct neural activity patterns in ALS patients, particularly in the motor regions, which are known to be affected early in disease course.[36,37] The clear separation observed in the latent variable space supports the overall idea that ALS progression can be effectively tracked through neuroimaging markers, potentially aiding in early diagnosis and personalized treatment strategies.

Both the modelling of disease onset site and severity proved more effective when using functional connectivity patterns rather than functional activation maps. This insight suggests that network-level co-activation associated with voluntary movement is more informative for capturing disease stage in ALS than overall activation within the MI alone. This network-level sensitivity may also be the reason why the functional and structural disease-defining information only parts overlap. Prior studies have indicated that the functional connectivity profile in ALS patients is predictive of disease stage, however, those studies often focused on cognitive decline and associated network changes,[38] or investigated resting state networks only.[39,40] In an overlapping cohort of $n = 8$ patients, we show that disease-defining structural and network changes only partly overlap, which may either be due to functional changes being more sensitive and detectable earlier, or due to compensatory network alterations in response to degenerating structures. Only longitudinal analyses in a larger cohort will uncover the mechanistic reason for this effect.

The result that functional connectivity changes are decreased compared to controls in King Stage 1, are increased in King Stage 2 and are decreased again King Stage 3 provides a further indication that functional network changes in MI are highly sensitive to disease progression.[41] This aligns with a study using MEG recordings from early-diagnosed ALS patients during speech tasks, which found greater sensory correlations and beta band connectivity in ALS patients compared to healthy controls.[42] This suggests that ALS patients exhibit increased functional connectivity in early stages of the disease to compensate for an initial decline in connectivity by recruiting additional networks as support architecture. The later decline in connectivity could then signal more severe disease stages with more pronounced myelin loss, where this compensation strategy fails. For translational applications, this could imply that focusing on maintaining this initial compensation strategy at a high level, i.e. focusing on preventing the decline in connectivity that is observed at later disease stages, may be a strategy to slow down disease progression. This finding is also in line with existing literature[43] that suggests early compensatory mechanisms in ALS, where the brain attempts to maintain motor function despite ongoing neurodegeneration.

With respect to the a/topographic functional architecture of ALS, our definition of 'topography' is based on earlier structural investigations of an overlapping patient group (with two new patients added in this study), which revealed that the first-affected body part shows higher iron accumulation in deep layers of MI compared to the later-affected regions in MI.[5] With this definition, a 'topographic' functional signature would show disease-defining features specifically in earlier-affected compared to later-affected regions of MI, following the deep layer iron accumulation. On the other hand, an atopographic functional signature could also be driven by stronger functional changes in newly-affected areas of MI and would indicate that disease-defining functional features are not necessarily most pronounced in the most clinically-affected body part. This assumption is based on the observation that the accumulation of nQSM in ALS (potentially reflecting calcium) is specifically pronounced in low-myelin borders of MI, which are located between body part areas of MI,[5] and that we detected generally lower myelination of the face area with ageing, indicating vulnerability of this region.[33] Our investigation reveals that regions first affected by ALS exhibit lower group (i.e. ALS versus control) classification accuracy compared with non-first affected regions in MI when using functional activation time series. This suggests that functional activation in the first-affected regions may not fully capture the early pathological changes driving ALS progression. Interestingly, the stronger classification accuracy observed in non-first affected regions likely reflects the progression to second or third affected body parts, as indicated by higher King stages. These non-first affected regions may exhibit more pronounced functional alterations, potentially due to advanced pathology resulting from later disease stages. The higher classification accuracy in these regions shows the importance of considering functional activation patterns over time as ALS progresses.

In contrast, the structural changes observed in previous studies, such as higher iron accumulation in the deep layers of MI in first-affected regions in these patients,[5] suggest that early ALS pathology can also be captured through structural imaging. In an exploratory analysis, we compared disease-defining information between structural (QSM) and functional (ECM) information and found that the patterns were only partly overlapping. This indicates that whereas structural information may provide information about local changes in iron, calcium and/or protein accumulation, the disease-defining functional information acts at the network level and includes compensatory mechanisms driven by other brain areas. However, our findings are limited by the absence of direct data on spinal cord and brainstem involvement or second motor neuron degeneration, which could significantly impact both functional activation and connectivity patterns. Future studies incorporating these regions and combining functional and structural markers in a larger cohort of patients may provide a more comprehensive understanding of ALS progression with respect to the interaction between the local and network level. Critically, the calcium accumulation in patients was specifically high in the low-myelin borders in MI that separate distinct body part areas[6] and that are assumed to be connected to different, non-topographic functional networks compared to the body part areas in MI.[44] This pattern of results hence indicates that disease-defining network changes do not necessarily overlap with the earliest-affected body parts and the hotspots of iron accumulation. In order to successfully track disease progress and to investigate the effect of medication, an accompanying mapping of functional network changes is therefore to be recommended based on our results.

We also show that both disease onset site and severity can best be captured by the foot and face areas in MI, rather than the hand area. The significant differences in weight distribution across different regions of the primary motor cortex further support this finding. This regional specificity could be due to the differential vulnerability of motor neurons in these regions to ALS-related pathologies such as iron accumulation.[45,46] In a recent study,[5] found that the hand region in MI in older adults shows less age-related iron accumulation compared to regions representing other body parts, arguing that the hand region is potentially less vulnerable compared to other areas in MI to effects of ageing.[5] This resilience could explain why the hand region displays fewer functional alterations, thus making it a less effective marker for classification in ALS. Another possibility is that hand dysfunction is detected earlier

behaviourally due to the very high level of hand dexterity in humans. This finding is also consistent with the fact that bulbar impairment is linked to shorter survival in ALS.[47] More pronounced changes in bulbar activity could serve as a more sensitive marker for overall disease aggressiveness and progression compared to other body parts.

Conclusion

In conclusion, this study demonstrates the potential of using rSRM and PLSR in combination with 7T-fMRI for uncovering the functional correlates of ALS progression and onset even in small patient samples. Our findings provide critical insights into the disease's atopographic patterns and highlight the importance of the face/tongue and foot regions in disease assessment, hinting towards their potential as biomarkers for tracking disease onset and progression. Given the functional disease-defining information was more pronounced on the network level and only partially overlapped with local structural disease-defining information, our study also highlights the benefits of combined structural and functional (i.e. multimodal) assessments of ALS pathology using ultra-high field MRI. These results pave the way for future research aimed at improving the diagnosis and management of ALS through advanced neuroimaging techniques.

Supplementary material

Supplementary material is available at *Brain Communications* online.

Funding

This work was funded by the Deutsche Forschungsgemeinschaft (DFG) (MA 9235/3-1/SCHR 1418/5-1 (501214112)), SFB 1436 Z02 (Project-ID 425899996), and the Else Kröner Fresenius Stiftung: 2019-A03.

Competing interests

The authors report no competing interests.

Data availability

fMRI/MRI data will be made available by the first author upon request. The extracted structural data from patients and controls is available at https://github.com/alicianorthall/In-vivo-Pathology-ALS/blob/main/ALS_Data.xlsx

Code availability

All code used for PLSR-based functional data analysis is available at: https://github.com/avinashkalyani/ALS_PLSr

References

1. Al-Chalabi A, Hardiman O, Kiernan MC, Chiò A, Rix-Brooks B, van den Berg LH. Amyotrophic lateral sclerosis: Moving towards a new classification system. *Lancet Neurol*. 2016;15(11):1182-1194.
2. Norris F, Shepherd R, Denys E, *et al.* Onset, natural history and outcome in idiopathic adult motor neuron disease. *J Neurol Sci*. 1993;118(1):48-55.
3. Ravits JM, La Spada AR. ALS motor phenotype heterogeneity, focality, and spread. *Neurology*. 2009;73(10):805-811.
4. Kollewe K, Münte TF, Samii A, Dengler R, Petri S, Mohammadi B. Patterns of cortical activity differ in ALS patients with limb and/or bulbar involvement depending on motor tasks. *J Neurol*. 2011;258(5):804-810.
5. Northall A, Doehler J, Weber M, *et al.* Multimodal layer modelling reveals in vivo pathology in amyotrophic lateral sclerosis. *Brain J Neurol*. 2024;147(3):1087-1099.
6. Kuehn E, Dinse J, Jakobsen E, *et al.* Body topography parcellates human sensory and motor cortex. *Cereb Cortex*. 2017;27(7):3790-3805.
7. Filippi M, Basaia S, Canu E, *et al.* Changes in functional and structural brain connectome along the Alzheimer's disease continuum. *Mol Psychiatry*. 2020;25(1):230-239.
8. Dan T, Kim M, Kim WH, *et al.* Uncovering structural-functional coupling alterations for neurodegenerative diseases. In: Greenspan H, Madabhushi A, Mousavi P, *et al.*, eds. *Medical image computing and computer assisted intervention—MICCAI 2023*. Springer Nature Switzerland; 2023:87-96.
9. Kuehn E, Pleger B. Encoding schemes in somatosensation: From micro- to meta-topography. *NeuroImage*. 2020;223:117255.
10. Schreiber S, Northall A, Weber M, Vielhaber S, Kuehn E. Topographical layer imaging as a tool to track neurodegenerative disease spread in M1. *Nat Rev Neurosci*. 2021;22(1):68-69.
11. Kreitz S, Mennecke A, Konerth L, *et al.* 3T vs. 7T fMRI: Capturing early human memory consolidation after motor task utilizing the observed higher functional specificity of 7T. *Front Neurosci*. 2023;17:1215400.
12. Cosottini M, Donatelli G, Costagli M, *et al.* High-resolution 7T MR imaging of the motor Cortex in amyotrophic lateral sclerosis. *AJNR Am J Neuroradiol*. 2016;37(3):455-461.
13. De Reuck J, Devos D, Moreau C, *et al.* Topographic distribution of brain iron deposition and small cerebrovascular lesions in amyotrophic lateral sclerosis and in frontotemporal lobar degeneration: A post-mortem 7.0-tesla magnetic resonance imaging study with neuropathological correlates. *Acta Neurol Belg*. 2017;117(4):873-878.
14. Johns SLM, Ishaque A, Khan M, Yang YH, Wilman AH, Kalra S. Quantifying changes on susceptibility weighted images in amyotrophic lateral sclerosis using MRI texture analysis. *Amyotroph Lateral Scler Front Degener*. 2019;20(5–6):396-403.
15. Barry RL, Babu S, Anteraper SA, *et al.* Ultra-high field (7T) functional magnetic resonance imaging in amyotrophic lateral sclerosis: A pilot study. *NeuroImage Clin*. 2021;30:102648.
16. Fox MD, Greicius M. Clinical applications of resting state functional connectivity. *Front Syst Neurosci*. 2010;4:19.
17. Kalyani A, Contier O, Klemm L, *et al.* Reduced dimension stimulus decoding and column-based modeling reveal architectural differences of primary somatosensory finger maps between younger and older adults. *NeuroImage*. 2023;283:120430.
18. Turek JS, Ellis CT, Skalaban LJ, Turk-Browne NB, Willke TL. Capturing shared and individual information in fMRI data. In: *2018 IEEE International Conference on Acoustics, Speech and Signal Processing (ICASSP);* Calgary, AB, Canada. IEEE Press, 2018:826-830.
19. Krishnan A, Williams LJ, McIntosh AR, Abdi H. Partial least squares (PLS) methods for neuroimaging: A tutorial and review. *NeuroImage*. 2011;56(2):455-475.
20. McIntosh AR, Lobaugh NJ. Partial least squares analysis of neuroimaging data: Applications and advances. *NeuroImage*. 2004;23(Suppl 1):S250-S263.
21. Chen C, Cao X, Tian L. Partial least squares regression performs well in MRI-based individualized estimations. *Front Neurosci*. 2019;13:1282.
22. Mehmood T, Liland KH, Snipen L, Sæbø S. A review of variable selection methods in partial least squares regression. *Chemom Intell Lab Syst*. 2012;118:62-69.

23. Lohmann G, Loktyushin A, Stelzer J, Scheffler K. Eigenvector centrality mapping for ultrahigh resolution fMRI data of the human brain. *Published online December*. 2018;13:494732.
24. Van Roon P, Zakizadeh J, Chartier S. Partial least squares tutorial for analyzing neuroimaging data. *Quant Methods Psychol*. 2014;10(2):200-215.
25. Cedarbaum JM, Stambler N, Malta E, *et al.* The ALSFRS-R: A revised ALS functional rating scale that incorporates assessments of respiratory function. BDNF ALS Study Group (Phase III). *J Neurol Sci*. 1999;169(1–2):13-21.
26. Al-Chalabi A, Chiò A, Merrill C, *et al.* Clinical staging in amyotrophic lateral sclerosis: Analysis of edaravone study 19. *J Neurol Neurosurg Psychiatry*. 2021;92(2):165-171.
27. Balendra R, Jones A, Jivraj N, *et al.* Use of clinical staging in amyotrophic lateral sclerosis for phase 3 clinical trials. *J Neurol Neurosurg Psychiatry*. 2015;86(1):45-49.
28. Quinn C, Edmundson C, Dahodwala N, Elman L. Reliable and efficient scale to assess upper motor neuron disease burden in amyotrophic lateral sclerosis. *Muscle Nerve*. 2020;61(4):508-511.
29. Yushkevich PA, Piven J, Hazlett HC, *et al.* User-guided 3D active contour segmentation of anatomical structures: Significantly improved efficiency and reliability. *NeuroImage*. 2006;31(3):1116-1128.
30. Avants B, Tustison NJ, Song G. Advanced normalization tools: V1.0. *Insight J*. 2009; 2(365):1–35.
31. Fonov V, Evans AC, Botteron K, Almli CR, McKinstry RC, Collins DL. Unbiased average age-appropriate atlases for pediatric studies. *NeuroImage*. 2011;54(1):313-327.
32. Maintz JBA, Viergever MA. A survey of medical image registration. *Med Image Anal*. 1998;2(1):1-36.
33. Northall A, Doehler J, Weber M, Vielhaber S, Schreiber S, Kuehn E. Layer-specific vulnerability is a mechanism of topographic map aging. *Neurobiol Aging*. 2023;128:17-32.
34. Lohmann G, Heczko S, Mahler L, *et al.* Improving the reliability of fMRI-based predictions of intelligence via semi-blind machine learning. *bioRxiv*. [Preprint]. doi:10.1101/2023.11.03.565485
35. Lohmann G, Müller K, Bosch V, *et al.* LIPSIA–a new software system for the evaluation of functional magnetic resonance images of the human brain. *Comput Med Imaging Graph Off J Comput Med Imaging Soc*. 2001;25(6):449-457.
36. Thome J, Steinbach R, Grosskreutz J, Durstewitz D, Koppe G. Classification of amyotrophic lateral sclerosis by brain volume, connectivity, and network dynamics. *Hum Brain Mapp*. 2022;43(2):681-699.
37. Zhang Q, Ding Y, Zhang Y, *et al.* Early cortical alterations and neuropsychological mechanisms in amyotrophic lateral sclerosis. *NeuroImage Clin*. 2025;47:103809.
38. De Marchi F, Carrarini C, De Martino A, *et al.* Cognitive dysfunction in amyotrophic lateral sclerosis: Can we predict it? *Neurol Sci*. 2021;42(6):2211-2222.
39. Agosta F, Valsasina P, Absinta M, *et al.* Sensorimotor functional connectivity changes in amyotrophic lateral sclerosis. *Cereb Cortex*. 2011;21(10):2291-2298.
40. Metzger M, Dukic S, McMackin R, *et al.* Functional network dynamics revealed by EEG microstates reflect cognitive decline in amyotrophic lateral sclerosis. *Hum Brain Mapp*. 2024;45(1):e26536.
41. Notturno F, Croce P, Ornello R, Sacco S, Zappasodi F. Yield of EEG features as markers of disease severity in amyotrophic lateral sclerosis: A pilot study. *Amyotroph Lateral Scler Front Degener*. 2023;24(3–4):295-303.
42. Dash D, Teplansky K, Ferrari P, *et al.* Automatic detection of ALS from single-trial MEG signals during speech tasks: A pilot study. *Front Psychol*. 2024;15:1114811.
43. Schoenfeld MA, Tempelmann C, Gaul C, *et al.* Functional motor compensation in amyotrophic lateral sclerosis. *J Neurol*. 2005;252(8):944-952.
44. Gordon EM, Chauvin RJ, Van AN, *et al.* A somato-cognitive action network alternates with effector regions in motor cortex. *Nature*. 2023;617(7960):351-359.
45. Donatelli G, Costagli M, Cecchi P, *et al.* Motor cortical patterns of upper motor neuron pathology in amyotrophic lateral sclerosis: A 3 T MRI study with iron-sensitive sequences. *NeuroImage Clin*. 2022;35:103138.
46. Kwan JY, Jeong SY, Gelderen PV, *et al.* Iron accumulation in deep cortical layers accounts for MRI signal abnormalities in ALS: Correlating 7 tesla MRI and pathology. *PLoS One*. 2012;7(4):e35241.
47. Stegmann GM, Hahn S, Liss J, *et al.* Early detection and tracking of bulbar changes in ALS via frequent and remote speech analysis. *Npj Digit Med*. 2020;3(1):132.